Supplement of

Response of the link between the El Niño–Southern Oscillation (ENSO) and the East Asian winter monsoon to Asian anthropogenic sulfate aerosols

Zixuan Jia et al.

Correspondence to: Zixuan Jia (zx.jia@nuist.edu.cn)

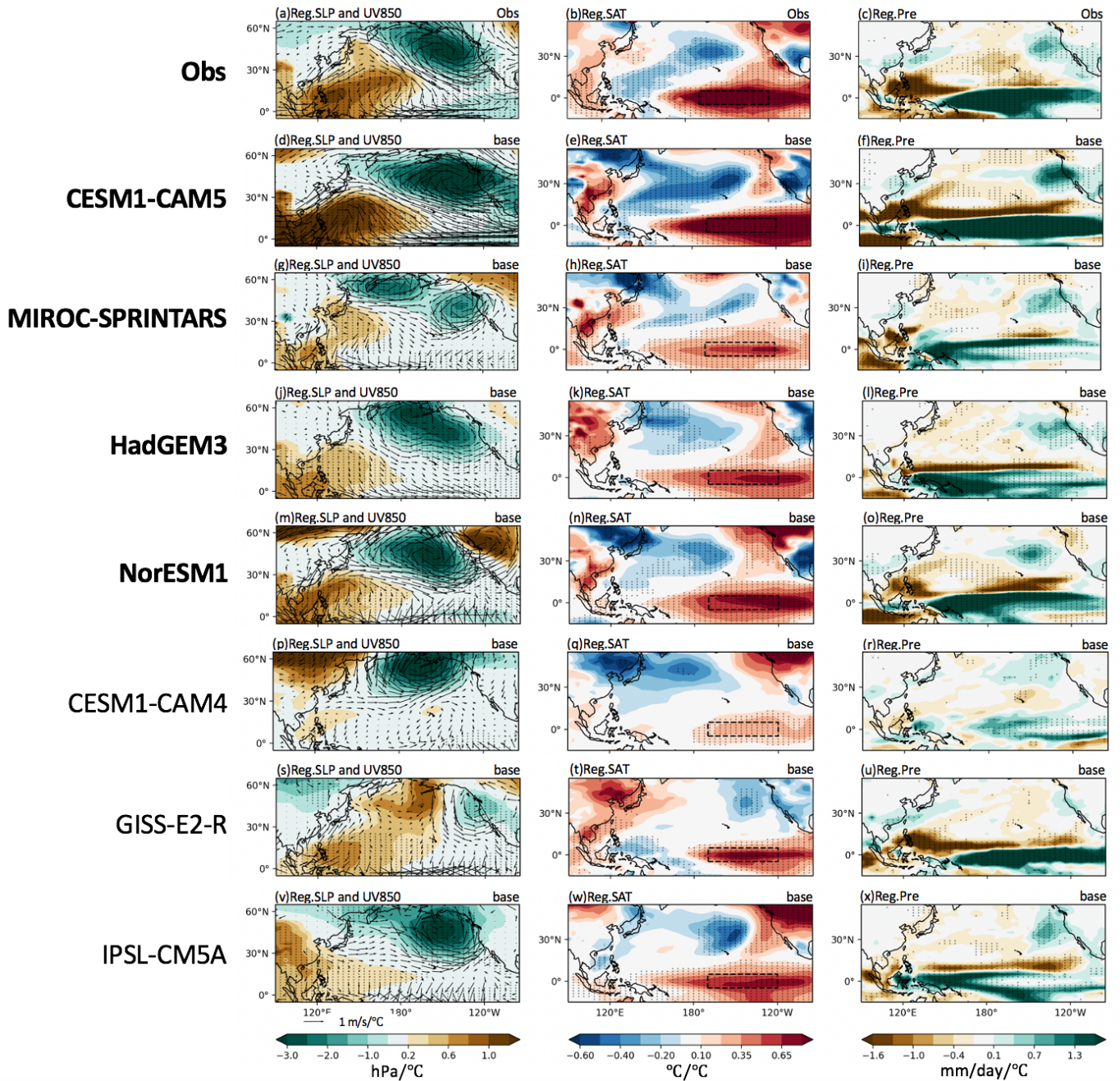# Supporting information

Figure S1. As in Figures 1a-c, and for (d-x) each model from the coupled baseline simulation in PDRMIP. Top four model names marked in bold are used in this study.
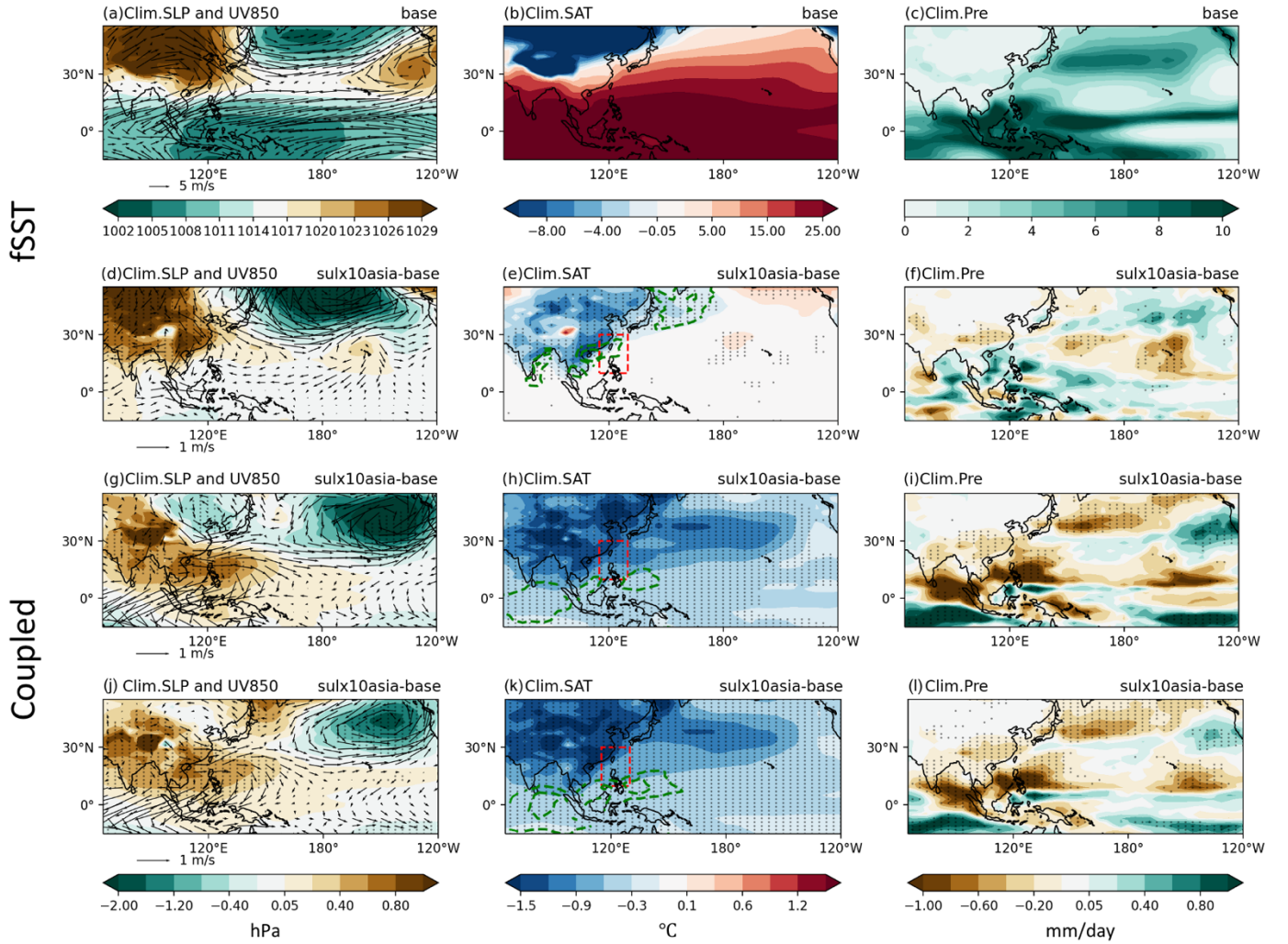
Figure S2. Top row: DJF multimodel mean of (a) sea level pressure (SLP; hPa, shading) and 850 hPa wind (UV850; m s^{-1}, vector), (b) surface air temperature (SAT, SST over the ocean, °C, shading), (c) precipitation (Pre, mm d^{-1}) from the PDRMIP fSST baseline simulations. Second row: DJF multimodel mean changes of (d) SLP and UV850, (e) SAT and 1000 hPa meridional wind (V1000, m s^{-1}, green contours, values plotted only when smaller than -0.1 m s^{-1}), (f) Pre between SUL×10Asia and baseline simulations in the PDRMIP fSST experiments. Bottom two rows: As panels (d-f), but for the PDRMIP coupled simulations during DJF for years 50-61 (g-i), for years 50-99 (j-l). Dotted regions indicate significant changes at the 95% level from the two-tailed Student's *t* test. The definition region of the EAWM index is marked by a red rectangle in the middle column (panels e, h and k).
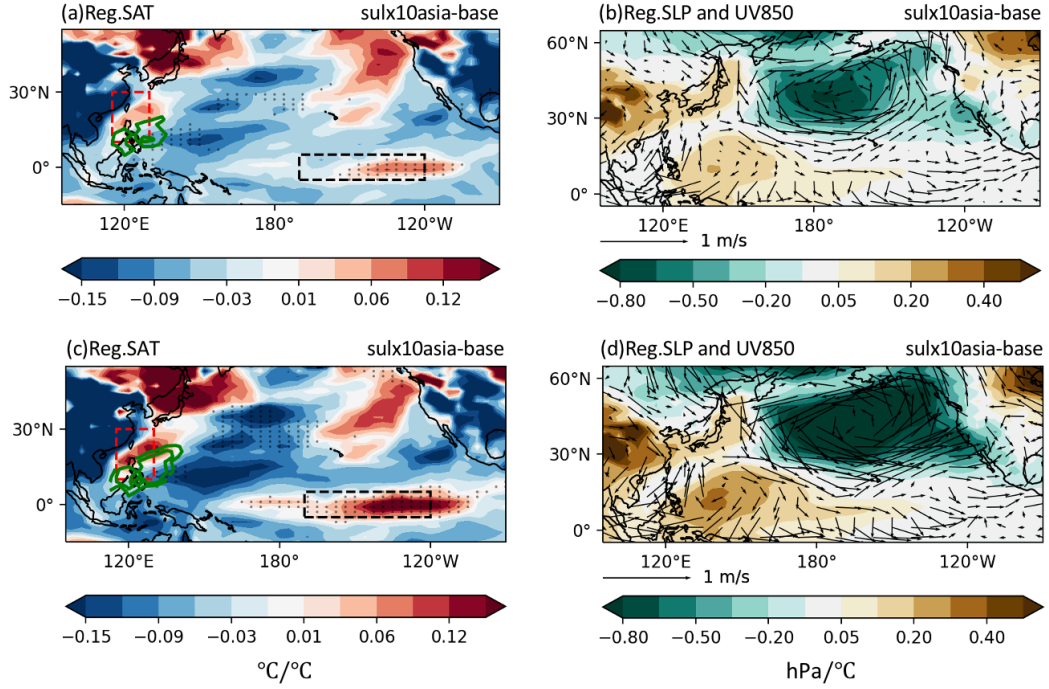
3

Figure S3. Differences in DJF multimodel regressions of (a, c) surface air temperature (SAT, SST over the ocean, °C, shading) and 1000 hPa meridional wind (V1000) over the broad East Asia (green contours, values plotted only when larger than 0.05 m s^{-1} °C^{-1}), (b, d) sea level pressure (SLP; hPa, shading) and 850 hPa wind (UV850; m s^{-1}, vector) onto the (a, b) Niño3 index, (c, d) Niño4 index between coupled SUL×10Asia and baseline simulations. Dotted regions represent differences that remain significant after false discovery rate (FDR) correction of *p-values* from two-tailed Student's *t*-test (Wilks et al., 2016). The definition regions of the EAWM index and the Niño3.4 index are marked by red and black rectangles respectively.
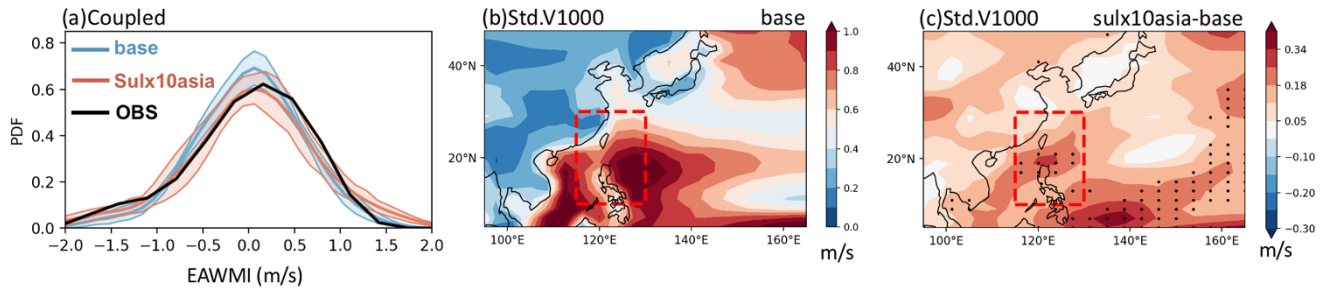
Figure S4. (a) Frequency distributions of the EAWM index from observations during DJF 1965-2014 (black curve) and (a) coupled simulations during DJF for years 50-99 in PDRMIP with multimodel-means (thick coloured curves) and the associated 95% confidence intervals (coloured shades). The confidence intervals are estimated from different models by using bootstrap resampling (e.g. Wang, 2001). (b) DJF multimodel mean standard deviations of V1000 (m s^{-1}) from coupled baseline simulations. (c) Differences in DJF multimodel mean standard deviations of V1000 (m s^{-1}) between coupled SUL×10Asia and baseline experiments. Dotted regions indicate significant differences at the 95% level from the two-tailed *F*-test. The definition region of the EAWM index is marked by a red rectangle.
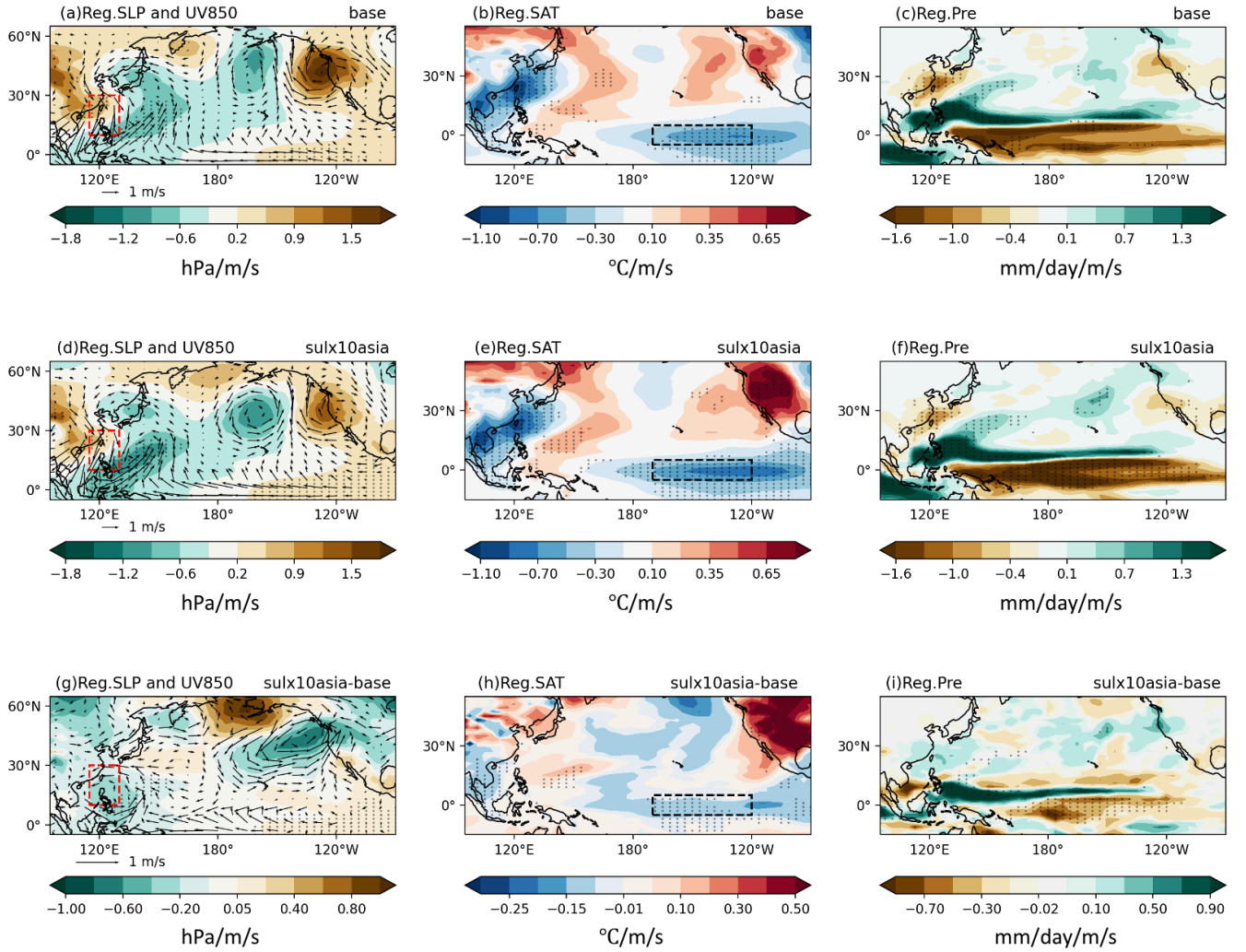
Figure S5. DJF multimodel mean regressions of (a)(d) SLP and UV850, (b)(e) SAT (SST over the ocean), (c)(f) Pre onto the EAWM index from coupled (a-c) baseline, (d-f) SUL×10Asia simulations in PDRMIP. Dotted regions indicate significant correlations at the 95% level from the two-tailed Student's t test. Differences in regressions of (g) SLP and UV850, (h) SAT (SST over the ocean), (i) Pre between coupled SUL×10Asia and baseline simulations. Dotted regions represent significant differences at the 95% level from the two-tailed Student's t test. The definition regions of the EAWM index and the Niño3.4 index are marked by red and black rectangles respectively.
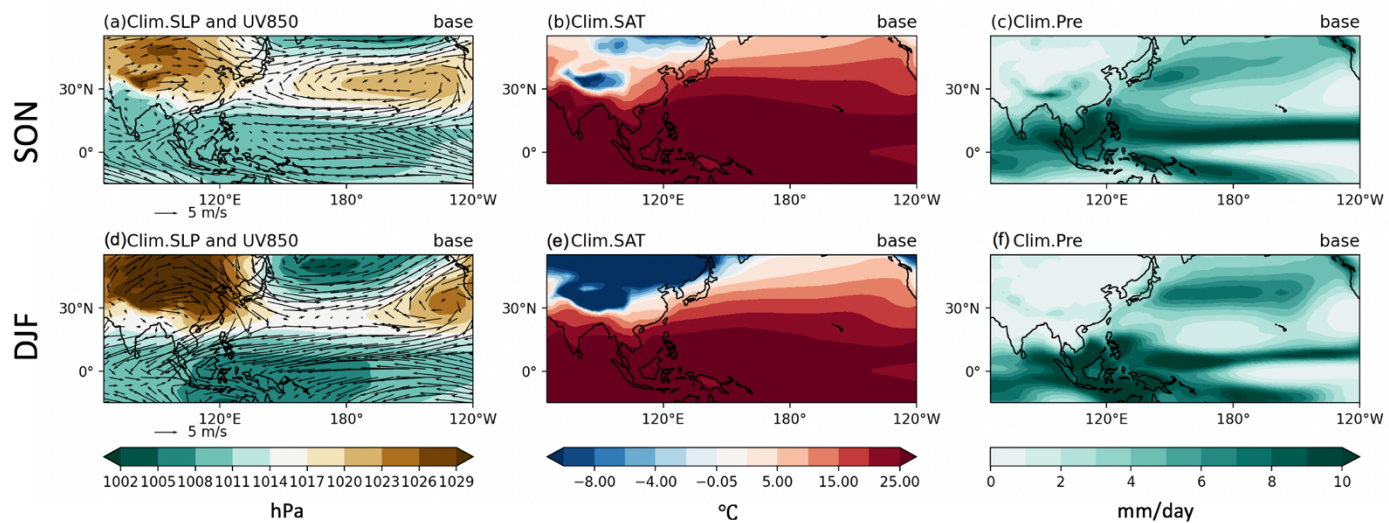
Figure S6. As in Figures S2a-c, but from coupled baseline simulations for (a-c) SON, (d-f) DJF.
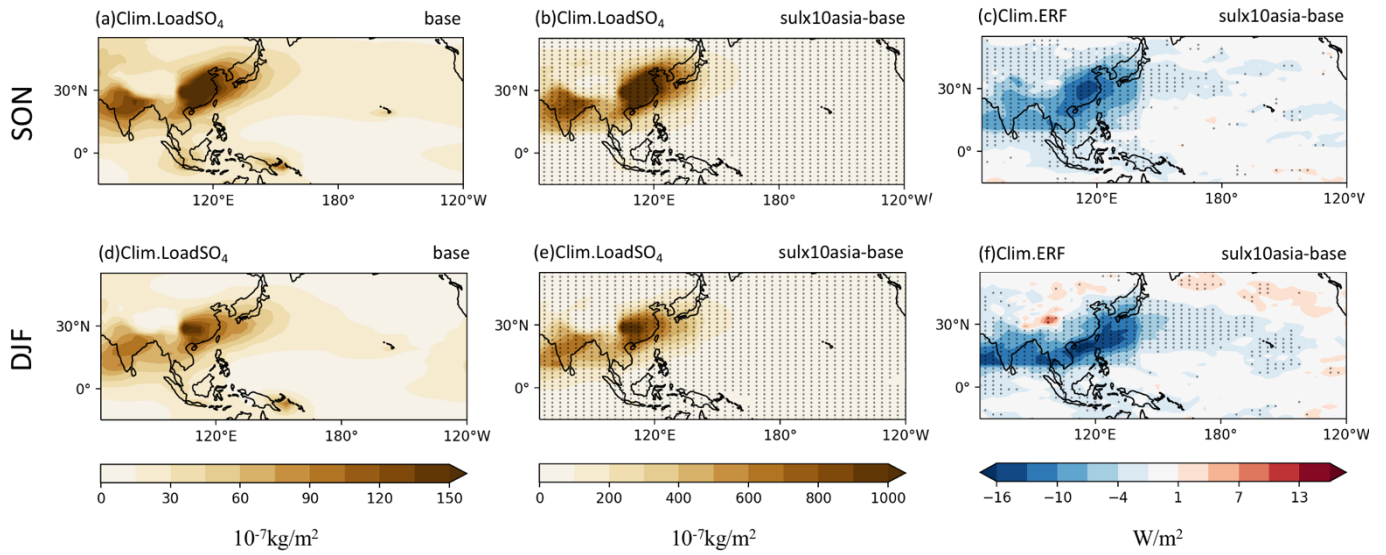
5

10

15

20

Figure S7. (a) SON, (d) DJF multimodel mean sulfate loading (10^{-7}kg/m^2) from the PDRMIP fSST baseline simulations. Changes in (b, e) sulfate loading and (c, f) effective radiative forcing (ERF, W/m^2) between fSST SUL×10Asia and baseline simulations in these two seasons. Dotted regions indicate significant changes at the 95% level from the two-tailed Student's t test.

5

10

15

20